

Molecular Physics

An International Journal at the Interface Between Chemistry and Physics

ISSN: 0026-8976 (Print) 1362-3028 (Online) Journal homepage: <http://www.tandfonline.com/loi/tmph20>

Excited state dynamics of new-type thermally activated delayed fluorescence emitters: theoretical view of light-emitting mechanism

Lili Lin, Jianzhong Fan, Lei Cai & Chuan-Kui Wang

To cite this article: Lili Lin, Jianzhong Fan, Lei Cai & Chuan-Kui Wang (2018) Excited state dynamics of new-type thermally activated delayed fluorescence emitters: theoretical view of light-emitting mechanism, *Molecular Physics*, 116:1, 19-28, DOI: [10.1080/00268976.2017.1362119](https://doi.org/10.1080/00268976.2017.1362119)

To link to this article: <https://doi.org/10.1080/00268976.2017.1362119>



Published online: 23 Aug 2017.



Submit your article to this journal [↗](#)



Article views: 68



View related articles [↗](#)



View Crossmark data [↗](#)

RESEARCH ARTICLE



Excited state dynamics of new-type thermally activated delayed fluorescence emitters: theoretical view of light-emitting mechanism

Lili Lin, Jianzhong Fan, Lei Cai and Chuan-Kui Wang

Shandong Province Key Laboratory of Medical Physics and Image Processing Technology, Institute of Materials and Clean Energy, School of Physics and Electronics, Shandong Normal University, Jinan, China

ABSTRACT

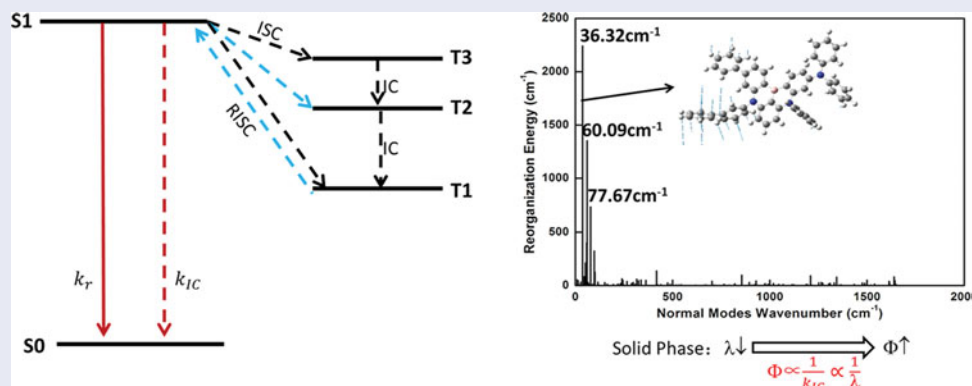
Excited state dynamics of two new-type thermally activated delayed fluorescence emitters (DABNA-1 and DABNA-2) synthesised based on multiple resonance effect is studied based on first-principles calculation, and their light-emitting mechanism is explored. The excited state dynamics combining with the adiabatic energy structure of several low-lying excited states indicates that three lowest triplet states are involved in the light-emitting process. The analysis of reorganisation energy indicates different performances for two molecules in solvent and in film. Our theoretical work provides rational explanation for experimental results, and also gives clear picture for light-emitting mechanism of these new-type molecules.

ARTICLE HISTORY

Received 9 May 2017
Accepted 25 July 2017

KEYWORDS

Thermally activated delayed fluorescence; reverse intersystem crossing; nonradiative decay; reorganisation energy; excited state dynamics



1. Introduction

Recently, thermally activated delayed fluorescent (TADF) emitters have attracted great attention, since their application in organic light-emitting diode (OLED) can dramatically enhance the exciton usage efficiency to nearly 100% by converting triplet excitons (T) to singlet excitons (S) effectively [1–4]. To realise the up-conversion of the triplet excitons, a small energy gap between the triplet and singlet excitons is required. One useful way to make a narrow S – T energy gap is to separate the highest occupied molecular orbital (HOMO) and the lowest unoccupied molecular orbital (LUMO) according to the equation $\Delta E_{st} = E_S - E_T = 2J$, where J is the exchange energy of the two unpaired electrons at the excited state ($J = \iint \Phi_L(1)\Phi_H(2)(\frac{e^2}{r_{12}})\Phi_L(2)\Phi_H(1)dr_1dr_2$, Φ_H and Φ_L represent the HOMO and LUMO wave functions). In

addition, one finds that artful connecting donor (D) and acceptor (A) groups by steric hindrance effect is the most frequently approach to obtain TADF molecules [5–9]. Nevertheless, the Stock shift of D–A type TADF molecules is increased because of enhancement of structure relaxation for their excited states. This effect results in broadening of electroluminescence peaks, which lowers displaying quality of OLED [10]. In order to solve this drawback, Hatakeyama *et al.* developed a new strategy for synthesising TADF molecules [11], namely, two new-type TADF molecules (DABNA-1 and DABNA-2) based on the multiple resonance effect were reported. These new-type molecules are not composed with D and A groups, but with nitrogen and boron atoms (shown in Figure 1). These two kinds of atoms exhibit opposite resonant effect, and significant separation of HOMO and LUMO can be formed. In the experiment results, significant TADF is

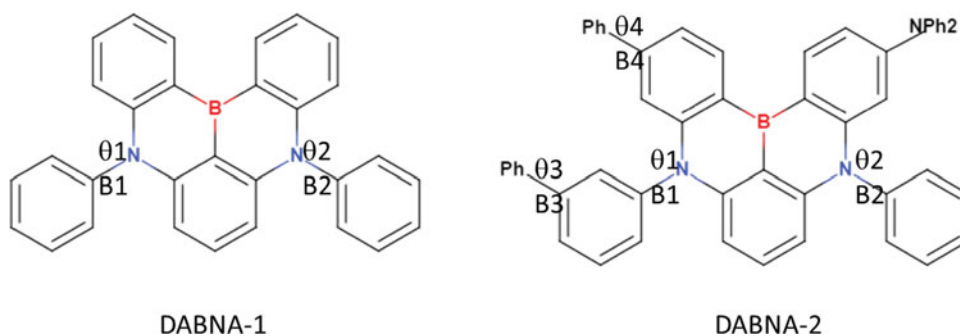


Figure 1. Schematic structures of DABNA-1 and DABNA-2.

found for both two molecules as emitters and the external quantum efficiency of the OLED with DABNA-2 as emitters is as high as 20.2%, which shows great potential for these new-type molecules applying in the OLEDs. However, one can note that the photoluminescence quantum yields (PLQY) for DABNA-2 in CH_2Cl_2 is 85%, while it is enhanced to 90% in mCBP film. However, no significant PLQY enhancement happens for DABNA-1 (89% in CH_2Cl_2 and 88% in mCBP film). Why two molecules show different performance in solution and film? What is the detail light-emitting process of the new-type TADF molecules? There is no explanation in the paper [11].

In this paper, we perform first-principles study on light-emitting mechanism of the two new-type TADF molecules by systematically studying the properties of excited states and also their dynamics. The results provide clear picture of light-emitting mechanism and also elucidate the reason that DABNA-2 molecule has larger PLQY in film than that in CH_2Cl_2 . Our theoretical study could provide valuable guides for understanding and designing high efficient TADF emitters.

2. Theoretical method

Excited state dynamics are studied based on first-principles calculations. The radiative decay rate (k_r) and nonradiative decay rate (k_{nr}) which includes internal conversion rate (k_{IC}) and intersystem crossing rate (k_{ISC}) are important factors for the excited state decay processes. For TADF-OLEDs, the reverse intersystem crossing (RISC) process plays a key role in achieving the high usage efficiency of excitons.

In our calculation, the radiative decay rate k_r is calculated using the Einstein spontaneous equation $k_r = \frac{f \Delta E_{fi}^2}{1.499}$, where f is the oscillator strength without unit and ΔE_{fi} is the vertical energy with the form of wave numbers (cm^{-1}) [12].

According to the Fermi's golden rule (FGR) and first-order perturbation theory, the nonradiative decay rate

can be written as follows:

$$K_{IC} = \frac{2\pi}{\hbar^2} \sum_{u,v} P_{iv} |H_{fu,iv}|^2 \delta(E_{iv} - E_{fu}) \quad (1)$$

where P_{iv} is the Boltzmann distribution function of the initial state, H is the interaction between two different Born–Oppenheimer states, and it contains two contributions as follows:

$$H \Psi_{iv} = H^{BO} \Phi_i(r, Q) \Phi_v(Q) + H^{SO} \Phi_i(r, Q) \Phi_v(Q) \quad (2)$$

where H^{BO} denotes the nonadiabatic coupling and H^{SO} is the spin-orbit coupling. When the small term $\partial^2 \Phi_i / \partial Q_{fi}^2$ is neglected, the first term reads:

$$\langle \Phi_f \Theta_{fu} | H^{BO} | \Phi_i \Theta_{iv} \rangle = \sum_l \langle \Phi_f \Theta_{fu} | (P_{fl} \Phi_i) (P_{fl} \Theta_{iv}) \rangle \quad (3)$$

In the equation above, l is the index of the normal mode and P_{fl} is the normal mode momentum operator of the l th normal mode in the final electronic state. So the internal conversion (IC) rate constant between two electronic states with same spin manifold can be written as:

$$K_{IC} = \frac{2\pi}{\hbar} \sum_{kl} R_{kl} Z_i^{-1} \sum_{vu} e^{-\beta E_{iv}} \langle \Phi_{fu} | P_{fk} | \Phi_{iv} \rangle \langle \Phi_{iv} | P_{fl} | \Phi_{fu} \rangle \delta(E_{iv} - E_{fu}) \quad (4)$$

Here, $R_{kl} = \langle \Phi_f | P_{fk} | \Phi_i \rangle \langle \Phi_i | P_{fl} | \Phi_f \rangle$ is the nonadiabatic electronic coupling. Further, the equation can be written as follows by applying the Fourier transform of the delta function:

$$K_{IC} = \sum_{kl} \frac{1}{\hbar^2} R_{kl} \int_{-\infty}^{\infty} dt [e^{i\omega_{if}t} Z_i^{-1} \rho_{IC}(t, T)] \quad (5)$$

Similarly, the intersystem crossing rate constant between two electronic states with different spin states

Table 1. Emission wavelength (nm) for DABNA-1 and DABNA-2 calculated using different functionals.

	HF%	DABNA-1	DABNA-2
O3LYP	11.61	463	503
B3LYP*	15	457	494
B3LYP	20	438	467
PBE0	25	421	445
MPW1B95	31	411	430
BMK	42	392	407
M062X	54	375	387
Exp[11]	—	462	470

can be written as:

$$K_{\text{ISC}} = \frac{1}{\hbar^2} \langle \Phi_f | H^{\text{SO}} | \Phi_i \rangle \int_{-\infty}^{\infty} dt [e^{i\omega_{if}t} Z_i^{-1} \rho_{\text{ISC}}(t, T)] \quad (6)$$

Both the methodology and application of this formalism can be found in Peng's and Shuai's work [13–16].

3. Computational details

Geometric optimisation and electronic structure calculation of DABNA-1 and DABNA-2 molecules are performed using the density functional theory (DFT). For the optimisation of excited states, the time-dependent density functional theory (TD-DFT) is used. The solvent effect is also included by using the polarisable continuum model (PCM) implemented in the *Gaussian 09* package [17]. In consistent with the experiment, the CH_2Cl_2 solution is adopted here. Specifically, the equilibrium solvation method is employed in both geometry optimisation and vibrational frequency calculation for singlet and triplet states involved in this paper. The nonequilibrium solvation method is used to obtain the vertical transition energies for both singlet and triplet states.

Although TD-DFT method is usually adopted for the calculation of excited states especially for medium and large organic systems, and the properties of excited state are found sensitive to functionals. Besides, some publications have shown that TD-DFT with nonhybrid functional always underestimates transition energies for charge-transfer (CT) states due to the neglecting of long-range Coulombic attraction between the separated electrons and holes. While time-dependent Hartree Fork (TD-HF) usually suffers from the so-called electron correlation problem and it may overestimate transition energies, it is found that the excited state calculation is largely depended on the percentage of HF exchange (HF%) in functionals for different molecules [18,19]. So the first job is to determine the optimal functional for each molecule. As shown in Table 1, through comparing with the experimental values, the emission wave length calculated with

the O3LYP and B3LYP functionals for DABNA-1 and DABNA-2, respectively, have good agreement with experimental counterpart. Thus, the O3LYP and B3LYP functionals with 6-311G(d) basis set is adopted in the latter calculations for DABNA-1 and DABNA-2, respectively. All the first-principles calculations are realised in the Gaussian 09 program. Moreover, the ISC and RISC rates are not only relevant to ΔE_{ST} but also proportional to the square of the spin-orbital coupling (SOC) between selected singlet and triplet states. The SOC coefficient can be obtained by *Dalton* package [20] and the normal mode analyses are performed by DUSHIN program [21]. Finally, the nonradiative decay rate from S1 to S0 and the ISC, RISC rate between selected singlet and triplet states can be calculated in MOMAP (Molecular Materials Property Prediction Package) which shows superiority in describing and predicting optical properties of polyatomic molecules [22].

4. Results and discussion

4.1. Molecular geometric structures and electronic structures

The geometry structures of DABNA-1 and DABNA-2 in the ground state (S0), S1 and T1 are compared as shown in Figure 2. It is shown that there is only a little variation between the S0 and S1, T1 for the DABNA-1 molecule. While significant change of dihedral angles can be found in the S0 and S1 or T1 for the DABNA-2 molecule. From Table 2, we can see that all the bonds have little change in three states of two molecules. The difference of the dihedral angles for DABNA-1 in three states is no larger than 0.3° . While, the dihedral angles θ_3 (0.3° – 78.1°) and θ_4 (1.6° – 17°) change quite significantly for three states of DABNA-2. The dihedral angles θ_1 and θ_2 in DABNA-2 have even larger variation than the angles in DABNA-1. All these parameters indicate that the introduction of the benzene and diphenylamine units make the molecule more flexible and easier to change when the molecule is excited.

The distribution of HOMO and LUMO as well as their energy gaps for two molecules are plotted in Figure 3. As shown in this figure, large overlap between HOMO and LUMO can be found for both two molecules, which predicts large dipole moments in both molecules. Based on our calculations, we find that the electric transition dipole moment (EDM) of S1 is 8.25D and 19.63D for DABNA-1 and DABNA-2, respectively, and the oscillator strength is 0.2325 and 0.5214 correspondingly. Comparing the HOMOs and LUMOs for two molecules, we can see that there is significant electron distribution on the boron atom in the LUMOs, while no electron

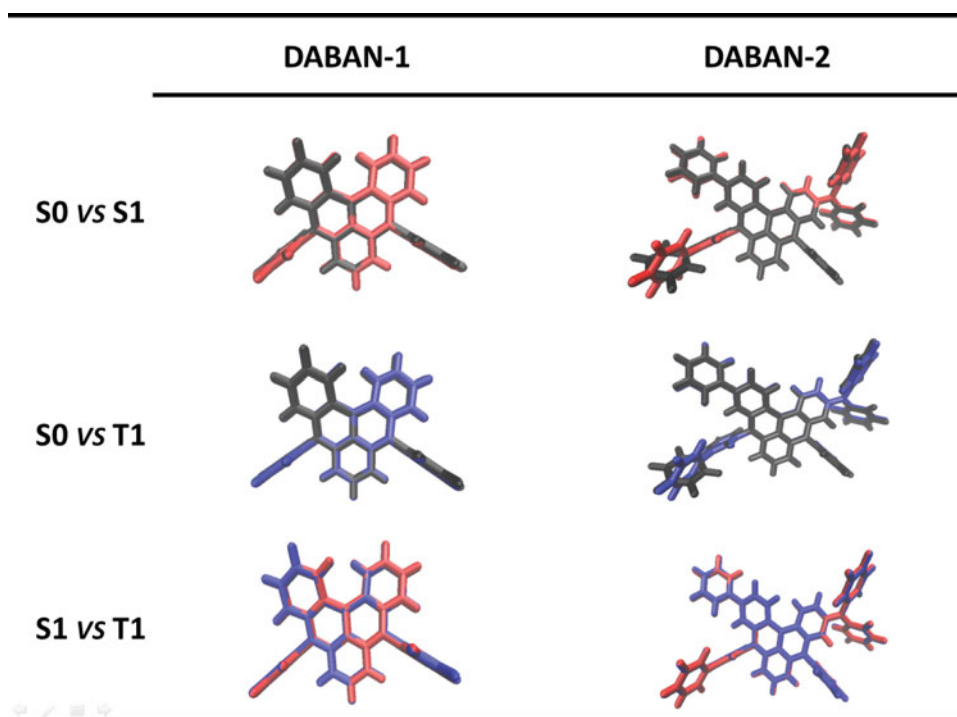


Figure 2. (Colour online) Intuitive comparison of geometry changes between S0 (black), S1 (red) and T1 (blue).

distribution on it in the HOMOs. The electron distribution on nitrogen atoms in the HOMOs is a little more than that in the LUMOs. For the HOMO and LUMO of DABNA-2, significant charge transfer from the benzene ring to the diphenylamine can be found besides obvious local excitation. The feature of hybrid local excitation and charge transfer in S1 which can induce both large fluorescent rate and also smaller S-T energy gap is quite rare [23]. Thus, the DABNA-2 shows great potential to be an excellent TADF emitter.

The vertical excitation (VE) and adiabatic excitation (AE) energies are calculated, respectively, for both molecules (see Figure 4). It can be seen that the energy structures for both molecules calculated with two methods are different. For DABNA-1, the energy level of T1 is lower than S1 and no additional energy level between them in both VE and AE landscapes. The S1-T1 energy gap is as large as 0.35 eV in the AE levels, which seems not favourable for RISC process. The S1-T1 energy gap calculated in VE picture is even larger. Thus, we deduce

that both the ISC and RISC processes should happen between the S1 and T1 states. For DABNA-2, three triplet energy levels T1, T2 and T3 are lower than S1 with the energy gap of 0.33, 0.11 and 0.07 eV, respectively, in the AE picture (see Figure 4(d)). In the VE picture, T2 is the closest to S1, and T3 is higher in energy than the S1 state. From the energy structure, we can deduce that the ISC process should happen between S1 and T1, T2 as well as T3, and the RISC process should mainly happen between S1 and T1. The T1-S1 energy gap in the AE picture is 0.33 eV, which is a little smaller than that in DABNA-1, but is still quite large for RISC in comparing with other TADF emitters [24].

4.2. Radiative and nonradiative decay rates

Based on the AE energy structure, we will calculate the decay rates for all the excited states involved. The short excited state lifetime of TADF materials (τ_{TADF}) is

Table 2. Torsion angles ($^{\circ}$) and bond lengths (\AA) for S0, S1 and T1 are listed, respectively. The labels in the table are shown in Figure 1.

	DABAN-1				DABNA-2							
	$\theta 1$	B1	$\theta 2$	B2	$\theta 1$	B1	$\theta 2$	B2	$\theta 3$	B3	$\theta 4$	B4
S0	88.9	1.442	88.9	1.442	88.5	1.444	89.2	1.444	—	1.486	38.6	1.486
S1	89.1	1.444	89.1	1.444	89.8	1.447	90.3	1.447	38.8	1.485	21.6	1.466
T1	89.2	1.444	89.2	1.444	89.3	1.447	90.2	1.447	39.0	1.486	23.2	1.468

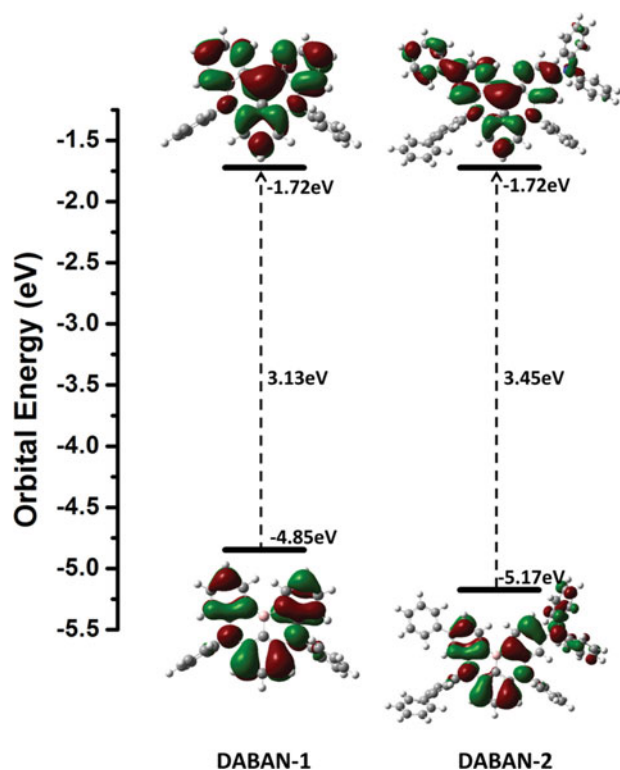


Figure 3. Calculated energy levels, energy gaps (in eV) and electron distribution of the HOMO and LUMO for DABNA-1 and DABNA-2 in ground state.

important to reduce the efficiency roll-off of TADF-OLEDs by suppression of the triplet–triplet annihilation (TTA) and singlet–triplet annihilation (STA). For TADF emitters, the rate constants of fluorescence (k_f), nonradiative decay from S1 (k_{IC}^S) and T1 (k_{nr}^T) as well as intersystem crossing (k_{ISC}) and reverse intersystem crossing (k_{RISC}) play key roles in dynamic process of excited states and also determine the lifetime of the excited states. As shown in Table 3, the radiation rate for DABNA-1 is $7.25 \times 10^7 \text{ s}^{-1}$, which is a little smaller than the fluorescent rate of DABNA-2 ($1.59 \times 10^8 \text{ s}^{-1}$). Both of them are in good agreement with the experimental results ($9.6 \times 10^7 \text{ s}^{-1}$ for DABNA-1 and $1.41 \times 10^8 \text{ s}^{-1}$ for DABNA-2). The IC rate for S1 of DABNA-2 is also larger than that of DABNA-1. In addition, the IC rate for the S1 state of both DABNA-1 and DABNA-2 are larger than the fluorescent rate, which is harmful for light-emitting. This

is maybe due to the insufficient description of the solvent effect by using the solvent model in our calculations. Nevertheless, we believe that the IC rates for both molecules will be smaller when the molecules are used in film. We will give detail analysis in next subsection. The ISC rate and the RISC rate between S1 and the triplet states involved are calculated. To calculate the (R)ISC rate, the spin-orbit coupling (SOC) between two states involved are needed. In Table 4, the SOC between S1 and some triplet states are listed. It can be seen that the SOC for both DABNA-1 and DABNA-2 are quite small in comparing with other organic molecules ($1\text{--}40 \text{ cm}^{-1}$) [25]. The SOC between S1 and T1 is about one order smaller than the SOC between S1 and T2 or T3. For DABNA-1, the ISC rate from S1 to T1 is even smaller than the rate from S1 to T2, although T2 is higher in energy than S1. From Table 4, we can see that the SOC between S1 and T2 is about eight times larger than that between S1 and T1. Based on the rate in Equation (6), the crossing rate from S1 to T2 should be 64 times larger than that from S1 to T1, supposing that the energy gap and other parameters are the same. From these parameters, we conclude that the SOC plays more important role than the energy gap between two states in the ISC process. For DABNA-2, the ISC rate from S1 to T2 is also larger than that from S1 to T3, although the energy gap between S1 and T3 is smaller than that between S1 and T2. It further indicates the importance of the SOC. To analyse the light-emitting mechanism, it is insufficient by only checking the energy structures of the states. One should always obtain the correct results by combining both the energy structures and also the decay rates of the states involved. Based on our calculations, we conclude that the intersystem process for DABNA-1 should mainly happen from S1 to T2, and quite little S1 states can convert to T3 or T1 states. Then T2 and T3 can quickly decay to T1, and the RISC happens mainly between T1 and S1. For DABNA-2, the ISC process also happens between S1 and T1, T2 and T3, and the ISC from S1 to T2 plays dominant role.

4.3. Huang-Rhys factor and reorganisation energy

As we all know, the nonradiative decay rate is closely related to the geometrical distortion between the emissive excited state and the ground state. Thus, the Huang-Rhys

Table 3. Calculated radiative and nonradiative rates of S1 as well as the ISC and RISC rates between singlet and triplet excited states for DABNA-1 and DABNA-2.

	$k_f (\text{s}^{-1})$ (S1 \rightarrow S0)	$k_{IC}^S (\text{s}^{-1})$ (S1 \rightarrow S0)	$k_{nr}^T (\text{s}^{-1})$ (T1 \rightarrow S0)	$k_{ISC} (\text{s}^{-1})$ (S1 \rightarrow T1)	$k_{RISC} (\text{s}^{-1})$ (T1 \rightarrow S1)	$k_{ISC} (\text{s}^{-1})$ (S1 \rightarrow T2)	$k_{RISC} (\text{s}^{-1})$ (T2 \rightarrow S1)	$k_{ISC} (\text{s}^{-1})$ (S1 \rightarrow T3)	$k_{RISC} (\text{s}^{-1})$ (T3 \rightarrow S1)
DABNA-1	7.25×10^7	9.11×10^7	3.00×10^2	5.03×10^3	6.68×10^2	1.36×10^4	3.73×10^5	1.00×10^4	6.78×10^4
DABNA-2	1.59×10^8	3.63×10^8	1.39×10^6	1.36×10^3	8.19×10^2	2.09×10^5	8.33×10^3	4.94×10^4	3.07×10^4

Table 4. Calculated spin orbit coupling constants (in cm^{-1}) between selected singlet and triplet excited states for DABNA-1 and DABNA-2 based on their optimised S1, T1, T2 and T3 structures, respectively.

Geometry	DABNA-1			DABNA-2		
	$\langle S1 H_{so} T1 \rangle$	$\langle S1 H_{so} T2 \rangle$	$\langle S1 H_{so} T3 \rangle$	$\langle S1 H_{so} T1 \rangle$	$\langle S1 H_{so} T2 \rangle$	$\langle S1 H_{so} T3 \rangle$
S1	0.009	0.073	0.053	0.005	0.047	0.025
T1	0.009	—	—	0.007	—	—
T2	—	0.055	—	—	0.053	—
T3	—	—	0.024	—	—	0.055

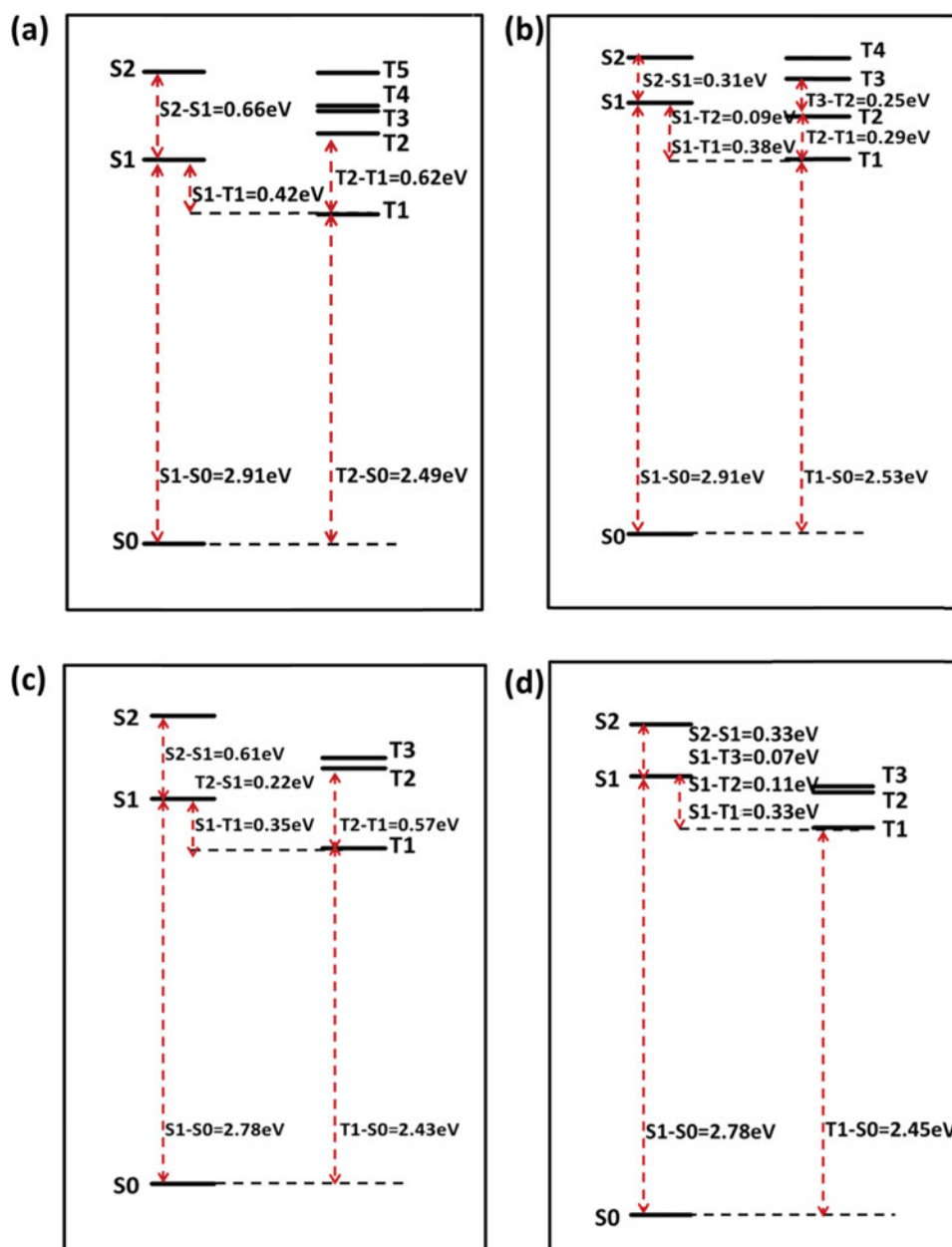


Figure 4. Energy landscape of vertical excitation energy for (a) DABNA-1 and (b) DABNA-2 as well as adiabatic excitation energy for (c) DABNA-1 and (d) DABNA-2.

factor (S_j) and reorganisation energy (λ_j) are calculated to elucidate the relationship between molecular rigidity and nonradiative decay process.

$$S_j = \frac{1}{2\hbar} w_j K_j^2$$

$$\lambda_{gs} = \sum_{j \in gs} \lambda_j = \sum_{j \in gs} \hbar w_j S_j$$

$$\lambda_{es} = \sum_{j \in es} \lambda_j = \sum_{j \in es} \hbar w_j S_j$$

$$\lambda = \lambda_{gs} + \lambda_{es}$$

Here, K_j is the displacement for the mode j between the equilibrium geometries of S_0 and S_1 , and w_j is the vibration frequency of mode j . All these quantities can be obtained by DUSHIN program. One should note that λ_j is the reorganisation energy contributed by mode j . The schematic diagram for reorganisation energy is illustrated in Figure 5. E_{abs}^{peak} is the absorption energy for S_1 , E_{em}^{peak} is the fluorescence energy and ΔE_{ad} is the AE energy of S_1 . The reorganisation energies are listed in Table 5. It is found that both λ_{gs} and λ_{es} for DABNA-2 are larger

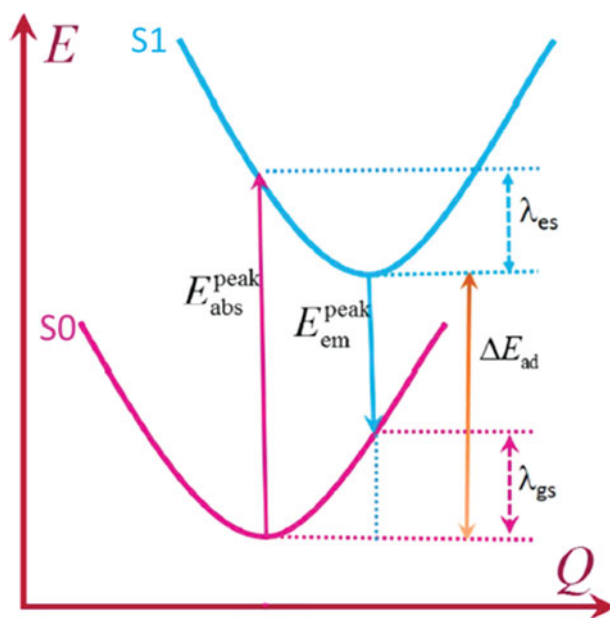


Figure 5. Sketch of the potential energy surfaces (PESs) for ground and excited states.

than these of DABNA-1. It is owing to that the introduction of the benzene ring and the diphenylamine make the DABNA-2 more flexible, which can induce significant

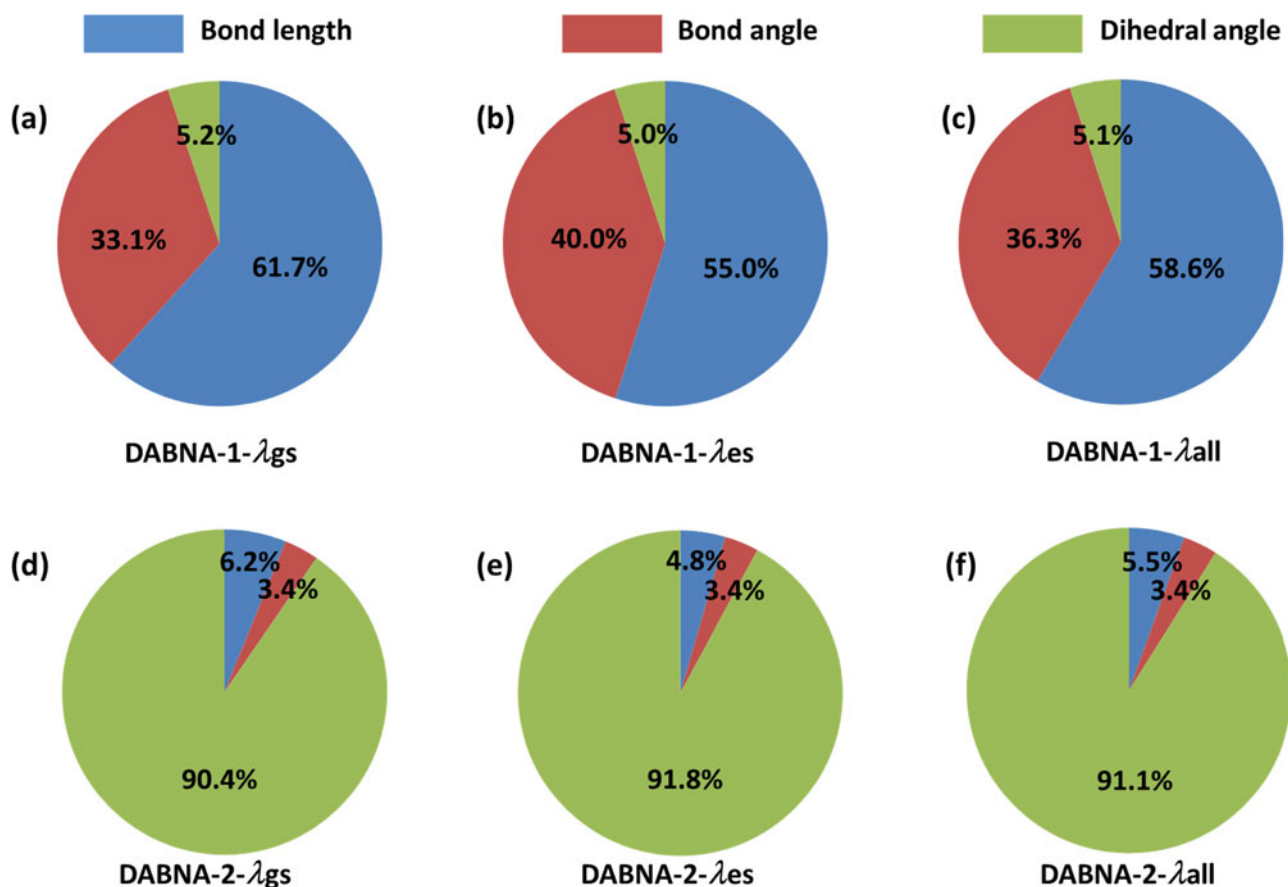


Figure 6. Contribution to the reorganisation energy of ground state (λ_{gs}), excited state (λ_{es}) and both two states (λ_{all}) from bond lengths, bond angles and dihedral angles of DABNA-1 and DABNA-2, respectively.

Table 5. Contributions from bond lengths, bond angles and dihedral angles to the reorganisation energy of DABNA-1 and DABNA-2 in ground state (λ_{gs}), excited state (λ_{es}) and the sum of both (λ_{all}). (Unit: meV).

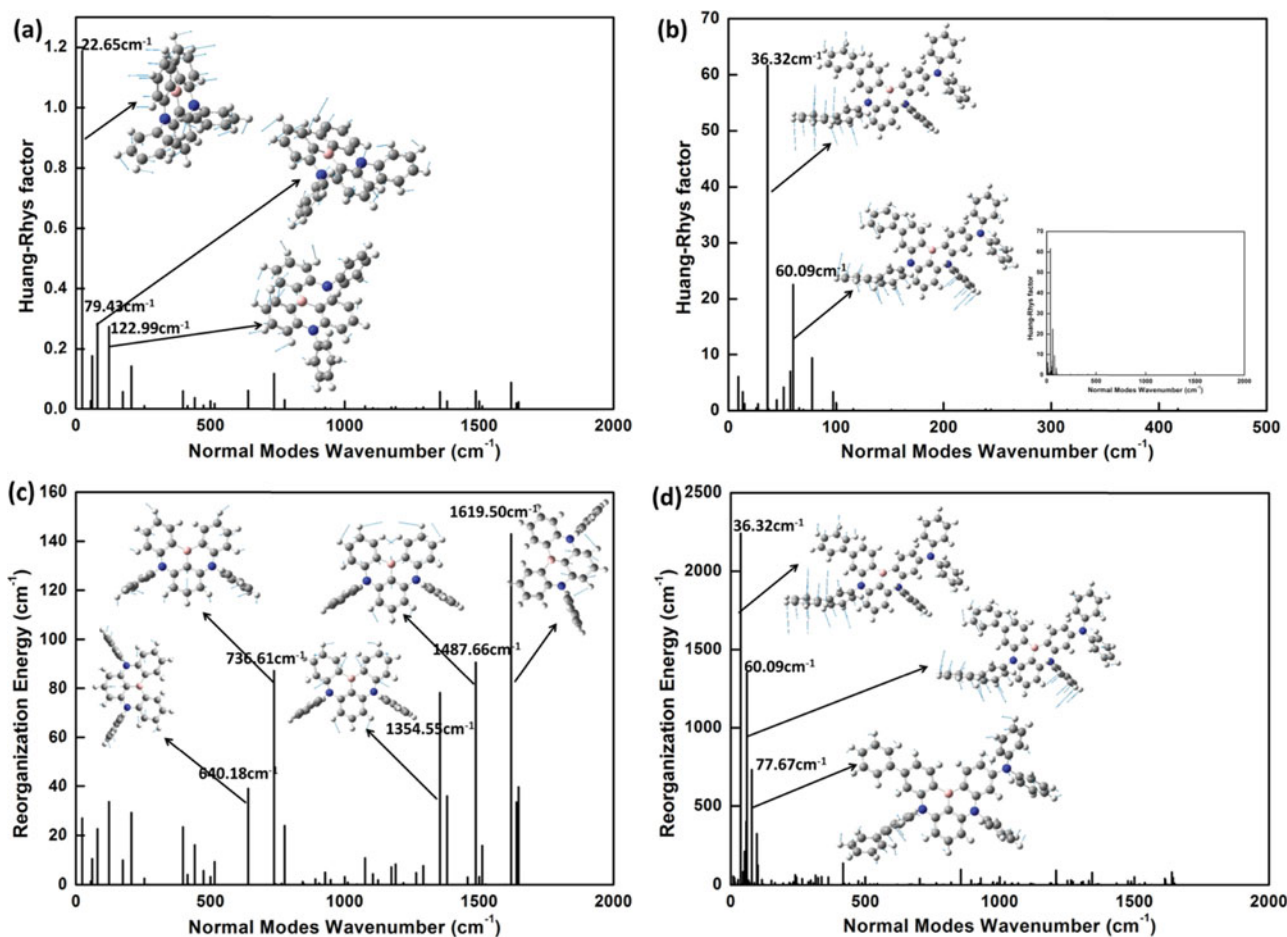
	DABNA-1				DABNA-2			
	Bond length	Bond angle	Dihedral angle	Total	Bond length	Bond angle	Dihedral angle	Total
λ_{gs}	61.7	33.1	5.2	100.0	58.9	32.3	858.8	950.0
λ_{es}	49.5	36.0	4.5	90.0	43.2	30.6	826.2	900.0
λ_{all}	111.2	69.1	9.7	190.0	102.1	62.9	1685.0	1850.0

relaxation when the molecule is excited or in decay process.

To confirm our deduction, the reorganisation energies are projected onto the internal coordinate of the molecules, and the reorganisation energies contributed from bond length, bond angle and dihedral angle are summarised in Figure 6 and Table 5. For DABNA-1, it is noted that the contribution to the total reorganisation energy from bond lengths, bond angles and dihedral angles are 111.2, 69.1 and 9.7 meV, respectively. It is obvious that the main contribution to λ_{all} comes from the bond length (58.6%), which is mainly due to its

rigidity. While for DABNA-2, the reorganisation energy from bond lengths, bond angles and dihedral angles are 102.1, 62.9 and 1685 meV, respectively, which shows that 91.1% reorganisation energy are from the dihedral angles.

The reorganisation energy and the Huang–Rhys factor versus the mode frequency are shown in Figure 7. It can be seen that the HR factors of DABNA-2 are about 52 times larger than those of DABNA-1. For DABNA-1, the reorganisation energies are mainly contributed by high frequency modes ($>500\text{cm}^{-1}$) which is associated with C–C stretching vibrations (inset in Figure 7(c)).

**Figure 7.** Calculated HR factors for (a) DABNA-1 and (b) DABNA-2 as well as reorganisation energies for (c) DABNA-1 and (d) DABNA-2. Vibration modes with large contribution to HR factors and reorganisation energy are shown as insets.

This finding is consistent with the results obtained in the internal coordinate projection of reorganisation energy. For DABNA-2, the modes with large reorganisation energies all appeared in low frequency region, e.g., 36.32, 60.09 and 77.67 cm⁻¹. These modes are assigned to the twisting motions of the side phenyl rings, and the normal mode displacement vectors are shown in Figure 7(d).

Based on the analysis of the reorganisation energy, we can understand the reason that the PLQY of DABNA-2 in film is greatly enhanced in comparison with the efficiency in the solvent. In film, the DABNA-2 molecules have more compact packing than that in solvent, thus the intermolecular interaction becomes stronger. The twisting motion of the side phenyl rings attached in the DABNA-2 molecule can be effectively hindered. Consequently, the reorganisation energy contributed from the vibration modes with low frequencies will be reduced. The vibration relaxation is suppressed and the nonradiative rate can be significantly decreased. As we know, the quantum efficiency of OLED is determined by four factors: $\eta_{\text{int}} = \gamma * \eta_1 * \eta_2 * \eta_{\text{out}}$ with γ is the exciton generation efficiency, η_1 is the exciton usage efficiency, η_2 is the fluorescent efficiency and η_{out} is the out coupling parameters. η_2 can be expressed as $\eta_2 = \frac{k_r}{k_r + k_{nr}}$, where k_r is the fluorescent rate and k_{nr} is the nonradiative rate. It is obvious that the fluorescent efficiency can be enhanced by reducing the nonradiative rate. It is also easy to understand why the efficiency of DABNA-2 in film is greatly increased due to the suppression of the nonradiative process. Of course, the nonradiative rate in solvent can be smaller if the surrounding effect can be described more correctly. Actually, we should perform investigation of the light-emitting properties of the molecules in solid state by using the QM/MM method as our former work [26]. However, there are no crystal structures for these molecules available which can be the reliable reference for the packing pattern of the molecules in solid state. Consequently, we can only give a deduction here that the nonradiative process can be suppressed, according to our experience and also other references [27,28].

5. Conclusions

In summary, the light-emitting mechanism of two new-type TADF molecules DABNA-1 and DABNA-2 are studied systematically based on first-principles study. The DABNA-2 molecule becomes more flexible than the DABNA-1 molecule due to the introduction of the benzene and diphenylamine units. Significant charge transfer character is found for the S1 state of DABNA-2, and large oscillator strength is also obtained. Based on the analysis of the adiabatic energy structure and the decay rates of several low-lying excited states, we know that three lowest

triplet excited states are involved in the ISC process for both molecules, while the RISC process takes place from T1 to S1. By projecting the reorganisation energy on the internal coordinates and decomposing it on the vibration modes, we find the reorganisation energy of DABNA-2 mainly comes from the vibration modes in low frequency regions with the twisting motion of the side phenyl rings. As the vibration modes with low frequencies are easy to be hindered in the solid state, the nonradiative process can be effectively suppressed and high PLQY for DABNA-2 in film is obtained than that in CH₂Cl₂. However, the reorganisation energy of DABNA-1 is mostly contributed by the vibration modes with high frequencies which involve the C–C stretching modes. This motion is difficult to be suppressed in solid state. Thus, there will be little difference for the nonradiative decay rate of DABNA-1 in CH₂Cl₂ and in mCBP film. So, the PLQY should have no significant change for DABNA-1 in CH₂Cl₂ and in mCBP film. Our theoretical results provide rational explanation for the reason that the quantum efficiency of DABNA-2 in film or in OLED is significantly enhanced, and detailed analysis of the excited state dynamics also provides a clear picture of the light-emitting mechanism.

Acknowledgments

This work is supported by the National Natural Science Foundation of China (Grant Nos. 11374195 and 21403133). Thanks to the supporting of Taishan Scholar Project of Shandong Province and the Scientific Research Foundation of Shandong Normal University. Thanks to the supporting of the Promotive Research Fund for Excellent Young and Middle-aged Scientists of Shandong Province (grant number BS2014CL001) and the General Financial Grant from the China Postdoctoral Science Foundation (grant number 2014M560571). Great thanks to Professor Yi Luo, Professor Zhigang Shuai and Qian Peng for their helpful suggestion. Thanks to Professor Yingli Niu for his great help in the usage of MOMAP.

Disclosure statement

No potential conflict of interest was reported by the authors.

Funding

National Natural Science Foundation of China [grant number 11374195], [grant number 21403133]; Promotive Research Fund for Excellent Young and Middle-aged Scientists of Shandong Province [grant number BS2014CL001]; General Financial Grant from the China Postdoctoral Science Foundation [grant number 2014M560571].

References

- [1] H. Uoyama, K. Goushi, K. Shizu, H. Nomura, and C. Adachi, *Nature* **492**, 234 (2012).

- [2] Q.S. Zhang, J. Li, K. Shizu, S.P. Huang, S. Hirata, H. Miyazaki, and C. Adachi, *J. Am. Chem. Soc.* **134**, 14706 (2012).
- [3] K. Yoshida, T. Matsushima, H. Nakanotani, and C. Adachi, *Org. Electron* **31**, 191 (2016).
- [4] Y. Wada, K. Shizu, S. Kubo, T. Fukushima, T. Miwa, H. Tanaka, C. Adachi, and H. Kaji, *Appl. Phys. Express* **9**, 032102 (2016).
- [5] S. Hirata, Y. Sakai, K. Masui, H. Tanaka, S.Y. Lee, H. Nomura, N. Nakamura, M. Yasumatsu, H. Nakanotani, Q. Zhang, K. Shizu, H. Miyazaki, and C. Adachi, *Nat. Mater.* **14**, 330 (2015).
- [6] J.Z. Fan, S. Qiu, L.L. Lin, and C.K. Wang, *Chinese. J. Chem. Phys.* **29**, 291 (2016).
- [7] L. Lin, Z. Wang, J. Fan, and C. Wang, *Org. Electron.* **41**, 17 (2017).
- [8] J.Z. Fan, L.L. Lin, and C.K. Wang, *Chem. Phys. Lett.* **652**, 16 (2016).
- [9] L. Cai, J.Z. Fan, L.L. Lin, and C.K. Wang, *Mol. Phys.* **115**, 809 (2017).
- [10] X. Shang, D. Han, M. Liu, and G. Zhang, *RSC. Adv.* **7**, 5055 (2017).
- [11] T. Hatakeyama, K. Shiren, K. Nakajima, S. Nomura, S. Nakatsuka, K. Kinoshita, J. Ni, Y. Ono, and T. Ikuta, *Adv. Mater.* **28**, 2777 (2016).
- [12] D. McCumber, *Phys. Rev.* **136**, A954 (1964).
- [13] Y. Niu, Q. Peng, C. Deng, X. Gao, and Z. Shuai, *J. Phys. Chem. A* **114**, 7817 (2010).
- [14] Y. Niu, Q. Peng, and Z. Shuai, *Sci. China, Ser. B: Chem.* **51**, 1153 (2008).
- [15] Q. Peng, Y. Yi, Z. Shuai, and J. Shao, *J. Am. Chem. Soc.* **129**, 9333 (2007).
- [16] Q. Peng, Y.L. Niu, Q.H. Shi, X. Gao, and Z.G. Shuai, *J. Chem. Theory. Comput.* **9**, 1132 (2013).
- [17] M. Frisch, G. Trucks, H. Schlegel, G. Scuseria, M. Robb, J. Cheeseman, G. Scalmani, V. Barone, B. Mennucci, and G. Petersson, *Gaussian 09*, revision D. 01 (Gaussian, Inc., Wallingford, CT, 2009).
- [18] S. Huang, Q. Zhang, Y. Shiota, T. Nakagawa, K. Kuwabara, K. Yoshizawa, and C. Adachi, *J. Chem. Theory. Comput.* **9**, 3872 (2013).
- [19] X. Tian, H. Sun, Q. Zhang, and C. Adachi, *Chinese. Chem. Lett.* **27**, 1445 (2016).
- [20] Dalton 2011, a Molecular Electronic Structure Program, 2011 see <http://www.daltonprogram.org>.
- [21] J.R. Reimers, *J. Chem. Phys.* **115**, 9103 (2001).
- [22] Z.G. Shuai, Q., Peng, Y.L. Niu, and H. Geng, MOMAP, a Free Andopen-source Molecular Materials Property Prediction Package; Revision 0.2.004 (Beijing, 2014). <http://www.shuaigroup.net>.
- [23] D. Hu, L. Yao, B. Yang, and Y. Ma, *Philos. T. R. Soc. A* **373**, 20140318 (2015).
- [24] D. Volz, *J. Photon. Energy.* **6**, 020901 (2016).
- [25] D. Beljonne, Z. Shuai, G. Pourtois, and J.L. Bredas, *J. Phys. Chem. A* **105**, 3899 (2001).
- [26] J. Fan, L. Cai, L. Lin, and C.K. Wang, *J. Phys. Chem. A* **120**, 9422 (2016).
- [27] N.L. Leung, N. Xie, W. Yuan, Y. Liu, Q. Wu, Q. Peng, Q. Miao, J.W. Lam, and B.Z. Tang, *Chemistry-Eur. J.* **20**, 15349 (2014).
- [28] C. Deng, Y. Niu, Q. Peng, A. Qin, Z. Shuai, and B.Z. Tang, *J. Chem. Phys.* **135**, 014304 (2011).